

Design of a Nested Sodium and Proton Array for 7 Tesla Knee Imaging

Ryan Brown¹, Guillaume Madelin¹, Riccardo Lattanzi¹, Gregory Chang¹, Ravinder R Regatte¹, Daniel K Sodickson¹, and Graham C Wiggins¹

¹Radiology, New York University School of Medicine, New York, NY, United States

INTRODUCTION: Sodium MRI has shown promise for osteoarthritis research, though it is limited at clinical field strengths (≤ 3 T) by intrinsically low signal-to-noise ratio (SNR). Ultra high field MRI (≥ 7 T) has been utilized to alleviate these limitations in musculoskeletal applications (1). A dual-nuclei coil with multiple receive channels represents a substantial benefit over a dual-nuclei volume coil because of improved sodium SNR while still facilitating proton B_0 shimming and co-registered proton anatomical images. To accomplish these goals, we implemented a nested sodium/proton array for 7T knee imaging with the following modules: 1) an eight channel sodium receive array for high SNR, 2) a detunable sodium transmit-receive birdcage coil primarily for sodium excitation, and 3) a four channel proton transmit receive array. In place of the traditional “trap” method to achieve dual resonance (2), the resonance structures of stand-alone proton and sodium coils were judiciously implemented to avoid interaction.

METHODS: *Eight Channel Sodium Receive Array* The key to improved sodium SNR was an array of eight receive-only rectangular coils with 8.8cm (50°) arc length such that they were symmetrically arranged around a 20.3cm diameter former and partially overlapped (3) in the azimuthal direction to reduce inductive coupling, and 15cm in length to cover knee cartilage over the typical desired range of 10 to 12cm. Coils were tuned and matched to 78.6MHz and 50Ω while loaded with a cylindrical phantom (11.5cm diameter, 1890mL water doped with 7.1g $\text{NaSO}_4 \cdot 6\text{H}_2\text{O}$ and 9.5g NaCl). A 700mA fuse was added to each coil to provide supplementary protection. Common mode coaxial currents were reduced using shielded cable traps tuned to the sodium and proton frequencies. Coil Q was measured in four settings: 1) in isolation, 2) in the presence of the eight-channel array, 3) in the presence of the aforementioned and the transmit sodium birdcage, and 4) in the presence of the aforementioned and the proton array. Coil noise as a percentage of total noise was calculated according to $1 - \sqrt{1 - (Q_{\text{loaded}}/Q_{\text{unloaded}})}$ (4).

Detunable Transmit Sodium Birdcage Coil: A high pass sodium birdcage coil was preferred for sodium transmit because its non-uniform high-order modes occur at frequencies well-below the proton resonant frequency. Dimensions of the transmit birdcage were based on trade-offs between high B_{1+} uniformity and high peak B_{1+} , while requiring that the birdcage fit coaxially around the sodium receive array former with minimal disturbance to the contralateral leg. A full-wave electromagnetic simulation based on Dyadic Green’s functions (DGF) (5) was utilized to guide the choice of birdcage dimensions by calculating the B_{1+} field in a uniform cylindrical sample (13cm diameter and electric properties of muscle at 78.6MHz) on main axis of candidate birdcages with a range of lengths and diameters. DGF calculations indicated that a birdcage with 25.4cm diameter and 20cm length provided sufficient peak B_{1+} and head-foot coverage in the targeted cartilage region, while also appropriate to construct given the anatomical and mechanical restrictions mentioned above. PIN diodes in series

with each rung and at the drive points were forward (reverse) biased to activate (deactivate) the birdcage during sodium transmit (sodium loop receive or proton transmit-receive).

Four Channel Proton Transmit-Receive Array: An array of four proton loops was constructed to provide adequate SNR in the knee articular cartilage with minimal disturbance to the sodium channel. Their geometry was chosen empirically given tradeoffs between high B_{1+} uniformity and coverage afforded by large coils, and low coupling between neighboring coils that favors small coils; coils were 3cm (arc length) \times 7cm (head-foot length) and positioned concentric to four sodium loops with azimuthal positions of 0° (anterior), 90° , 180° (posterior), and 270° . A relatively narrow conductor width of 0.2 cm was chosen to reduce shielding and eddy current loading of the sodium loops and birdcage. RF transmission was provided through a cascade of power splitters that divided the power into four equal parts with a phase shift equal to each coil’s azimuthal position. For RF receive, each coil was connected to a preamplifier via a PIN diode controlled transmit-receive switch with the appropriate length of coaxial cable for preamplifier decoupling. Detuning circuits were not necessary for the proton transmit-receive array.

Imaging Imaging was performed on two volunteers using a whole-body 7T scanner (MAGNETOM, Siemens) upon approved by our local IRB and with informed written consent from the volunteers. The dual-nuclei array was compared to two mono-nuclear transmit-receive birdcage coils (sodium: 20cm diameter and 17cm length, Rapid Biomedical; proton: 21cm diameter and 14cm length, Invivo Corp.) via SNR measurements in the same volunteer for each nuclei (GRE acquisitions; sodium: TE/TR/FA = 3.5ms/100ms/90°, $4.7 \times 4.7 \times 25\text{mm}^3$, scan time=8s; proton: TE/TR/FA = 4.1ms/200ms/20°, $0.9 \times 0.9 \times 3\text{ mm}^3$, scan time=51s; both: BW=260Hz/pixel, signal averages=1).

RESULTS: **Sodium** Sodium SNR for the dual-nuclei array was 10% greater in the phantom center and 130% greater in the periphery (Fig. 2). Notably, the proton array had a negligible effect on dual-nuclei sodium SNR. Similar SNR gains of 1.2 to 1.7-fold were seen in the articular cartilage (Fig. 3). Noise associated with a sodium coil in isolation was similar to that in situ with the complete dual-nuclei array (Table 1). As a secondary note, the mono-nuclear birdcage SNR was 34% greater than the detunable sodium birdcage due to its increased diameter and detuning diodes required to accommodate the receive array. Although the eight-channel array is the primary means for reception, receive capability is also available on the detunable sodium birdcage to provide a uniform image useful for sodium quantification. Diode detuning of the dual-nuclei sodium birdcage provided $>20\text{dB}$ of sensitivity isolation at 78.6MHz, while the detuned resonances did not approach 297.2MHz. The transmit voltage for 90° excitation with a 1ms hard pulse in the center of the phantom was 215v for the dual-nuclei sodium birdcage and 167v for the mono-nuclear sodium birdcage. **Proton** Compared to the mono-nuclear birdcage, the SNR for the dual-nuclei array was higher in the periphery but lower in the center (Fig. 4), while FWHM head-foot coverage and 90° transmit voltage was 8.9cm and 270v (dual-nuclei array), and 11.9cm and 190v (mono-nuclear birdcage).

DISCUSSION: A dual-nuclei sodium/proton array was demonstrated with substantial sodium SNR gain over a conventional mono-nuclear sodium birdcage. By managing the resonances of each module, the sodium receive channels were maintained in the most favorable form, without SNR-lowering circuitry that is commonly used in dual-tuned coils such as trap circuits or in-line PIN diodes. This approach resulted in sodium SNR gains of 1.2-1.7 fold *in vivo*. The presented dual-nuclei array additionally provided proton B_0 shimming and co-registered anatomical reference imaging capability while interaction with the sodium channel was negligible.

REF 1. Wang, et al. JMRI 2009. 2. Schnall, et al. JMR 1985. 3. Roemer, et al. MRM 1990. 4. Hayes and Axel. Med Phys 1985. 5. Lattanzi and Sodickson. MRM *in press*.

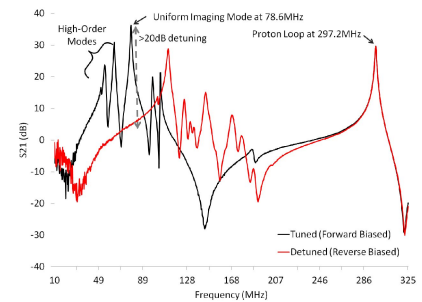


Fig. 1. Spectra of the tuned and detuned sodium bircage and a proton loop coil.

Table 1. Dual-nuclei array Q measurements.			
Coil	Setting	Q_{unloaded}	Q_{loaded}
Sodium loop	1	330	105
Sodium loop	2	260	85
Sodium loop	3	190	70
Sodium loop	4	180	70
Sodium bircage	4	110	55
Proton loop	4	205	155
			Noise (%)
			17
			18
			21
			22
			29
			51

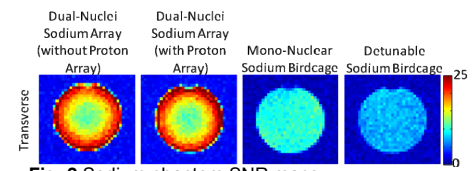


Fig. 2 Sodium phantom SNR maps.

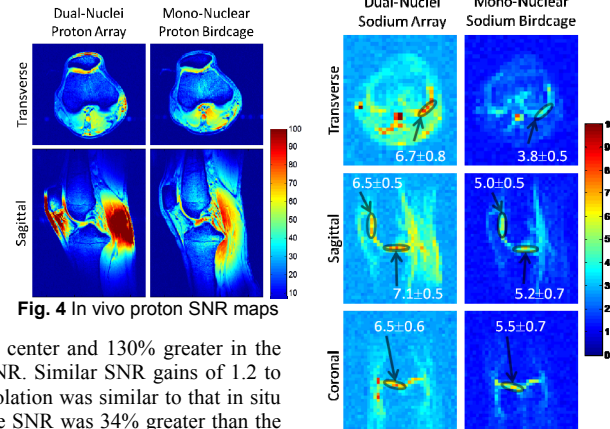


Fig. 3 In vivo sodium SNR maps